ON THE FEASIBILITY OF THERMOPLASTIC MATERIALS FOR MULTIFUNCTIONAL ENERGY STORAGE SOLUTIONS

A. Beutl[1*], Q. Jiang[2], H Kühnelt[1], and A. Bismarck[2]

[1] Center for Low-Emission Transport, AIT Austrian Institute of Technology GmbH, Vienna, 1210, Austria. * corresponding author (alexander.beutl@ait.ac.at)

[2] Institute of Material Chemistry and Research, University of Vienna, Währinger Strasse 42, Vienna, 1090, Austria

Keywords: thermoplastic materials, multifunctional energy storage, structural batteries, multifunctional composites

ABSTRACT

Multifunctional energy storage for use in the automotive or aeronautic field promises to resolve current limits in energy density, by providing energy storage without the penalty of additional weight. Reinforcing conventional battery systems and integration into composite structures allows to manufacture panels with multifunctional energy storage. The integrated batteries, though, are required to sustain similar mechanical stress at similar weights as the composite materials they are exchanged with. This requirement poses quite a challenge considering that conventional batteries are just a layup of three composite sheets (anode, cathode, and separator), soaked with a liquid electrolyte. Therefore, many attempts to improve the mechanical properties of battery layups have been conducted with mixed results. Especially the low mechanical strength of the electrolyte has been the focus of recent research.

In this work, PVdF-based thermoplastic materials are investigated for use in multifunctional energy storage cells and compared with thermoset materials. The morphological, electrochemical and mechanical properties of the prepared electrolyte films are investigated by physico-chemical methods and discussed for their application in multifunctional energy storage units. Vital challenges regarding processability, adhesion, and thermal stability, which are often neglected, are highlighted in this work.

1 INTRODUCTION

Multifunctional energy storage solutions are of upper most interest for the mobility sector, including both the aviation and automobile industry, as considerable overall weight savings are expected upon implementation. Several different integration studies have been conducted showing the potential of this upcoming technology. Nevertheless, a clear strategy on how to realize multifunctional electrical energy storage, especially at larger scale, has not been established yet. One promising approach is to adopt components of conventional energy storage systems, i.e. electrodes and electrolytes, and reinforce them with mechanically strong matrices to obtain multifunctional materials [1-3].

Regarding the three main battery components, i.e. cathode, anode, and electrolyte, the latter is the weakest link regarding mechanical strength. In conventional battery cells, the electrolyte is composed of a thin, porous separator soaked with a carbonate-based liquid electrolyte. The soaked separator shows even lower tensile strength compared to the dry one [4, 5]. In addition, negligible adhesion between the three components does not allow for effective load transfer and thus poses a risk for mechanical failure. Therefore, development of multifunctional energy storage must be accompanied with the development of suitable electrolyte layers. Currently, two streams of research can be distinguished in this regard. First, the liquid electrolyte is reinforced by addition of a mechanically strong porous network, which is cured only after assembly of the battery cell. After curing, a bicontinuous material is obtained, being composed of a percolating rigid thermoset polymer and a continuous liquid electrolyte phase [6]. These so called bicontinuous (structural) electrolytes have attracted a lot of attention and were often seen as the most promising choice for realizing multifunctional energy storage. They allow for the preparation of a rigid and dense electrolyte sheet with high Young's modulus. Usually epoxy-based or similar thermoset materials are used for this approach [7-11]. Although the separator layer yields promising

performance, the integration of the layer into a battery cell and especially the contact between the separator layer and the electrodes has not been sufficiently investigated.

Another line of research regarding electrolytes for multifunctional energy storage, focuses on homogenous mono-phasic systems, which are either prepared by reinforcing the liquid electrolyte with a gelling polymer [12-14], or by using polymer electrolytes without liquid component [15]. These electrolytes use thermoplastic materials, which on the one hand exhibit lower Young's moduli compared to their thermoset counterparts, but increased electrochemical performance and ease of processing. In addition, they can be readily used as adhesive layer between the two electrodes by application of a thermal joining process.

In this work thermoset and thermoplastic based electrolytes for use in multifunctional energy storage are prepared and compared based on several parameters including ionic conductivity, Young's modulus, and processability. The chemical interactions of the electrolyte components are highlighted and their impact on multifunctionality discussed.

2 EXPERIMENTALS

2.1 Materials and solvents

For all electrolyte films, an ionic liquid electrolyte is used. Lithium bis(trifluoromethanesulfonyl)imide (LiTFSI, 99.9 % extra-dry, 20 ppm max.), N-Propyl-N-methylpyrrolidinium bis(fluorosulfonyl)imide ($PYR_{13}FSI$, 99.9 %) and N-Propyl-N-methylpyrrolidinium bis(trifluoromethanesulfonyl)imide ($PYR_{13}TFSI$, 99.9 %) were all purchased from *Solvionic* and used as received. The chemicals were only opened inside an Ar-filled glovebox (O_2 < 0.1 ppm, H_2O < 0.1 ppm) and further used for preparation of the ionic liquid electrolytes (ILE). The compositions were adapted depending on the requirements of the added polymers. Preparation of the ionic liquid electrolyte was conducted inside the glovebox using an Al-bottle as container and a magnetic Polytetrafluoroethylene (PTFE)-coated stirring bar. Appropriate amounts of the LiTFSI salt were added to either $PYR_{13}TFSI$, $PYR_{13}FSI$ or a mixture of both and stirred for 16 hours at 80 rpm. The clear and colorless solutions were then transferred into a dry room (dew point around -50°C) and stored until further use.

For the thermoset based polymers, two commercial epoxy-based systems were employed, i.e. Araldite LY5052/ Aradur 5052 (Huntsman) and Araldite LY556/ XB3473 (Huntsman). For the thermoplastic based electrolytes Poly(vinylidene fluoride) (PVdF, Solef 5130, Solvay) and Poly(vinylidene fluoride-co-hexafluoropropylene) (PVdF-HFP, Sigma Aldrich, avg. Mn ~400k) were used. 1-Methyl-2-pyrrolidone (NMP, ≥99.8%, Carl Roth) was used as received for dissolution of the thermoplastic polymers.

2.2 Preparation of electrolyte films

Preparation of the electrolyte films was conducted in a dry room at a dew point around -50°C unless otherwise noted.

Araldite LY5052/ Aradur 5052 – first the Araldite component was weighed and put into a glass bottle. Then the Aradur hardener is added, aiming for a weight ratio of 38 wt.% with respect to the overall weight of the thermoset material (following the recommendations of the data sheet). Subsequently, the ionic liquid electrolyte (0.1 LiTFSI-0.3 $PYR_{13}TFSI$-0.6 $PYR_{13}FSI$ mol./mol.) was added. The composition of the ILE was adopted from a recent publication which reported on its promising performance [16]. Several samples with different amounts of ILE were prepared using 20 vol.%, 40 vol.%, 45 vol.%, 50 vol.%, and 60 vol.%. After mixing all components using a glass rod, the mixture was degassed under dynamic vacuum for 10 min to remove possible air-bubbles inside the solution. Then the mixture was cast onto Mylar foil using a variable doctor blade (50-500 µm). The cast film was then cured at room temperature for 24 h and further at 100°C for 4 h.

Araldite LY556/ XB3473 – first the Araldite component is weighed and put into a glass bottle, and the XB3473 hardener is added, aiming for a weight ratio of 23 wt.%, following the recommendations in the data sheet. Then the ILE (0.22 LiTFSI-0.78 $PYR_{13}TFSI$ mol./mol.) was added, and the mixture was

mixed using a glass rod. After degassing under dynamic vacuum for 10 min, the solutions were cast onto PTFE-coated plates using a mask for setting the thickness of the obtained films.

PVdF/PVdF-HFP – For the preparation of the gel electrolytes, first, the respective polymers were dissolved in NMP to obtain approx. 8-10 wt.% solutions. Appropriate amounts of these were further mixed with the ionic liquid using a planetary centrifugal mixer (THINKY ARE-250) at 600 rpm for 2 min. The polymer-to-ionic liquid ratio was held constant at approx. 66:34 by weight and 70:30 by volume for all samples, unless otherwise stated.

The obtained solutions were then cast onto glass plates and dried at 80°C for 48 hours. After drying, colorless opaque films were obtained. Due to evaporation of the solvent, pores forming in the electrolyte film cannot be avoided and a densification step is applied to remove them. Therefore, all samples were subjected to a calendering step using a hot-rolling press (MTI, MSK-HRP-01). The temperature was set to be close to the melting point of the polymer materials, i.e. 145°C for PVdF and to 120°C for PVdF-HFP. Thus, samples with various thicknesses could be prepared. Usually, the as-cast films showed thicknesses of 100-150 µm and the minimum thickness obtained by calendaring was around 30-50 µm. For densification, the electrolytes were sandwiched in-between two Kapton release films (50 µm thick) to avoid contamination of the instrument with the ionic liquid electrolyte.

2.3 differential scanning calorimetry and scanning electron microscopy

Differential scanning calorimetry (DSC) was conducted using a NETZSCH DSC 204 F1 Phoenix. A heating rate of 5 K/min was used and a temperature range of -30°C to 200°C for the thermoset samples, whereas 10 K/min and a range of 25°C to 200°C for the thermoplast samples. All measurements were conducted under protective N_2 atmosphere.

Scanning electron microscopy (SEM) was performed using a ZEISS Supra 40 electron microscope. An acceleration voltage of 3 kV was used. The sample films were mounted on sample holders under dry atmosphere (dry room, dew point ~-50°C) using Ag-paste. Cross-sections for the samples were manually cut using a scalpel. The samples were then transported to the microscope within a sealed container. The container was opened only for mounting the samples to the SEM instrument, which exposed them to air for around 30 s. Thus, contamination due to adsorbed moisture from the surrounding air could be limited to a minimum, however not fully prevented.

2.3 Electrochemical and mechanical testing

The electrolyte films were cut into circular shapes (18 mm diameter) and tested by potentiostatic electrochemical impedance spectroscopy (PEIS) to determine their ionic conductivity. The samples were put between two stainless steel electrodes using an ECC-Std setup (EL-CELL). An excitation potential of 10 mV and frequencies of 1 MHz to 0.1 Hz were applied. The PEIS measurements were conducted inside a climatic chamber at temperatures ranging from 30°C to 80°C. All measurements were conducted using a BIOLOGIC VSP potentiostat.

Mechanical tests were conducted using an Instron 4502 universal testing machine (Instron Instruments Ltd, Bucks, UK). The samples were punched into miniaturized dog-bone shapes of 30 mm x 2 mm. The thicknesses of the samples were in the range of 50 µm. At least three replicate tests were performed for each sample. Young's moduli were determined from the linear elastic region of the stress-strain curves obtained from the measurements and were defined as the maximum values of this region.

3 RESULTS AND DISCUSSION

3.1 processability and ionic conductivity

Processability of the electrolytes was evaluated for different amounts of the ILE. First samples using the Araldite LY5052/ Aradur 5052 system were prepared and analyzed. Figure 1 shows the prepared samples ranging from 20 vol.% to 60 vol.% ILE. At 20 vol.% of ILE rigid and clear films (cf. Figure 1a,b) could be produced. The color after curing turned slightly bluish, which was not observed for the thermoset polymer without the ILE. The ionic conductivity of this membrane was rather low at only $1 \cdot 10^{-7}$ S/cm. Similarly, the MacMullin number (N_M), i.e. the ratio between the ionic conductivity of the

pristine ionic liquid electrolyte ($3 \cdot 10^{-3}$ S/cm) and the electrolyte within the porous thermoset, was high amounting to M_N = 30000. Addition of 40-45 vol.% ILE, showed similar processability as for the sample with only 20 vol.% and thin electrolyte films of around 250 to 25 µm (cf. Figure 1c) could be obtained by simple tape casting. For these samples, dendritic structures could be observed within the thermoset matrix (cf. Figure 1d). Some components or reaction products during curing have formed and crystallized after thermal treatment. Additionally, some of the ionic liquid electrolyte could be observed on the surface of the electrolyte film as small droplets (cf. Figure 1e). The ionic conductivity could be increased by one order of magnitude to 1-$1.3 \cdot 10^{-6}$ S/cm, and the MacMullin number decreased to M_N = 3020-2270.

Figure 1: electrolyte samples using Araldite LY5052/ Aradur 5052 thermoset system as reinforcing agent. Samples using 20 vol.% (a,b), 40-45 vol.% (c-e), 50 vol.% (f-g), and 60 vol.% (h-i) are shown after curing.

Nevertheless, the obtained ionic conductivities were not high enough for feasible cell performance. Addition of even more ILE diminished the mechanical properties of the films after curing and samples using 50 vol.% ILE could not be removed from the substrate anymore without major damage and cracking (cf. Figure 1f,g). At 60 vol.% the electrolyte could not be properly cast anymore and a slush-like mixture rather than a cohesive film was obtained (cf. Figure 1h,i). Thus, the combination of Araldite LY5052/ Aradur 5052 and the ILE was deemed as not suitable for application in multifunctional energy storage systems.

Therefore, another commercial thermoset was applied, i.e. Araldite LY556/ XB3473. Again, samples with different ILE amounts were prepared and analyzed. For this system, the polyester (Mylar) foil, which was used as substrate for tape casting of Araldite LY5052/ Aradur 5052 samples was not suitable as the adhesion of this thermoset was too high and the prepared samples could not be removed after curing. The same behavior was observed for polyimide (Kapton) foils (cf. Figure 2a,b). Therefore, PTFE coated plates were used as substrate for the Araldite LY556/ XB3473 samples. However, due to the high surface tension of the cast mixtures, inhomogeneous layers were obtained (cf. Figure 2c). Therefore, the electrolyte mixtures were sandwiched in-between two PTFE coated plates using a polyester mask to set the thickness for the electrolyte (cf. Figure 2d). The electrolyte samples were of opaque and milky color, whereas the pristine thermoset was brownish clear.

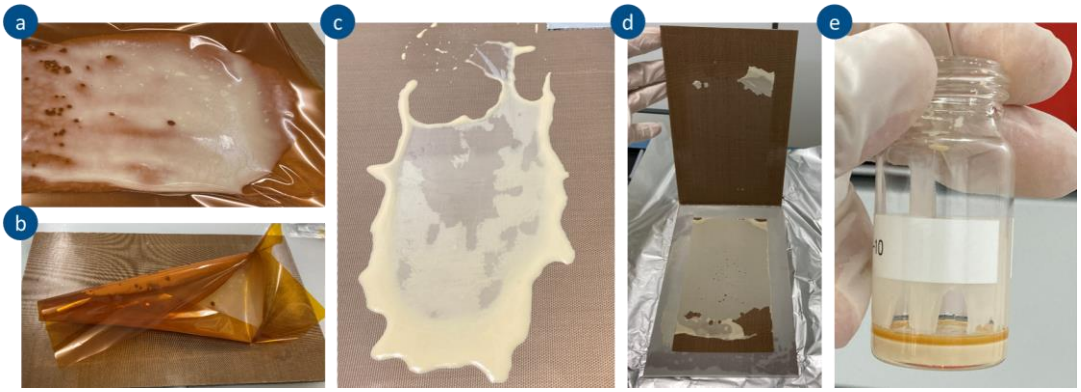

Figure 2: electrolyte samples using Araldite LY556/ XB3473 thermoset system as reinforcing agent. Samples using 40-50 vol.% (a-c), 70 vol.% (d-e) are shown after curing.

For samples using ≤40 vol.% ILE, no ionic conductivity could be recorded by PEIS as the internal resistance was too high. Only at ILE amounts of 50 vol.%, ionic conductivities of $5 \cdot 10^{-7}$ S/cm were obtained and M_N of 5970. Increasing the ILE amount to 60 vol.% increased the ionic conductivity considerably to $1 \cdot 10^{-5}$ S/cm and the MacMullin number to 235. In addition, acceptable mechanical properties made handling of the prepared films feasable. A further increase in the ILE content to 70 vol.% increased the ionic conductivity to $9 \cdot 10^{-4}$ S/cm and M_N = 3.3. However, the mechanical properties of the film also decreased significantly and handling the film without cracking or breaking was difficult. The electrochemical performance, though, of these samples is well in line with commercial separators for which M_N values of 5-10 are observed [17].

The thermoplastic samples showed good processability and ILE contents of 60 vol.% and 70 vol.% were prepared using PVdF and PVdF-HFP. After drying a slightly and highly opaque electrolyte film was obtained for samples using PVdF and PVdF-HFP, respectively (cf. Figure 3a,b). As no clear films were obtained, highly porous electrolyte films were assumed and thus a hot-calendering step was applied to the electrolyte films. Thereafter, clear and colourless electrolyte films were obtained for all samples (cf. Figure 3c). The ionic conductivity of samples using 70 vol.% ILE showed promising ionic conductivities of $7 \cdot 10^{-4}$ S/cm and $1 \cdot 10^{-3}$ S/cm for the PVdF and PVdF-HFP based electrolyte films, respectively. Samples using PVdF but only 60 vol.% ILE showed ionic conductivities of only $3 \cdot 10^{-4}$ S/cm.

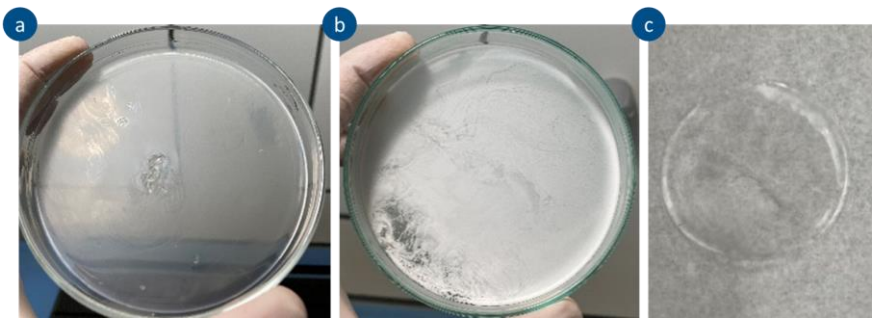

Figure 3: electrolyte samples after drying using a, PVdF and b, PVdF-HFP thermoplastic polymers and 70 vol.% of ILE. After hot-calendering, transparent films (c) are obtained.

Regarding processability, the brittle nature of the thermoset materials, as well as the difficult processing when aiming for thin electrolyte sheets (≤50 µm), makes them less attractive for multifunctional electrolytes than thermoplast containing electrolytes. The simple processing of the latter renders them superior regarding application in battery cells, as currently established processing methods (e.g. tape casting, hot calendering) can be readily adopted from conventional battery production. Furthermore, due to the thermoplast nature, electrode and electrolyte layers can be easily joined together applying a thermal post-treatment of the assembled battery cells.

3.2 SEM and thermal analysis

For further analysis of the samples, scanning electron microscopy and thermal analysis by DSC was conducted. In Figure 4, cross sections of different thermoset-based electrolyte layers are depicted. For the pristine material without any addition of ILE, a dense monolith is obtained as depicted in Figure 4a. Addition of 60 vol.% ILE results in the formation of a porous polymeric network into which the ILE can penetrate. Primary particles showing diameters of around 1 µm seem to be fused together during the curing process, building up the porous scaffold. Therefore, rather high ionic conductivities were obtained, and the mechanical stability was high enough for feasible handling of the electrolyte films. Further increase of the ILE content to 70 vol.% leads to an increase in the size of the primary particles to >2 µm and the particles seem to be isolated rather than connected. Thus, low mechanical stability was obtained for these samples. When the ionic liquid of the ILE was changes from $PYR_{13}TFSI$ to a mixture of $PYR_{13}TFSI$ and $PYR_{13}FSI$, a quite different morphology was observed. For this sample, a bone-like structure could be seen, showing a percolating network which itself is composed of a porous structure. The inner pores, however, seem to be closed and the ILE within is not able to contribute to the ionic conductivity of the electrolyte film. This complex behaviour and the dependency of the thermoset matrix on the quality of the ILE allows to assume a strong interaction between the thermoset precursor materials and the ILE.

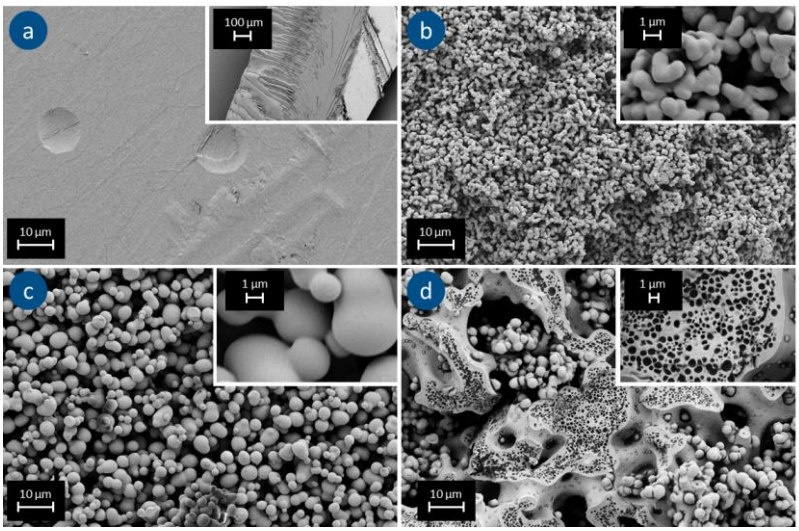

Figure 4: SEM micrographs of cross-sections obtained from a, pristine Araldite LY556/ XB3473 thermoset material after curing, b, the same material mixed with 60 vol.% 1M LiTFSI in $PYR_{13}TFSI$, c, with 70 vol.% 1M LiTFSI in $PYR_{13}TFSI$, d, with 60 vol.% of 1M LiTFSI in a mixture of $PYR_{13}TFSI$+$PYR_{13}FSI$.

Although the cross-sections of the thermoset electrolyte layers showed a well-connected percolation network, which allows the ILE to fill the interconnected porous network, the surface of the electrolyte films seemed to be quite different. As shown in Figure 5, the surface layer of all electrolyte films showed a thermoset *skin* which did not exhibit any pores. This *skin-effect* inhibits proper ionic conduction and

needs to be addressed accordingly.

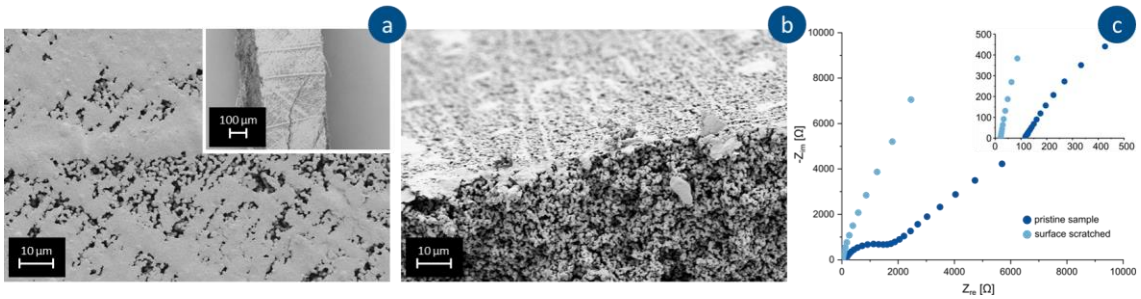

Figure 5: SEM micrographs of the surface layers of a, Araldite LY556/ XB3473 mixed with 60 vol.% 1M LiTFSI in $PYR_{13}TFSI$, b, with 60 vol.% of 0.5M LiTFSI in $PYR_{13}TFSI$. c, EIS measurements of sample depicted in (a) without any surface treatment and after scratching using a razor blade.

Indeed, if the surface of the thermoset electrolytes was scratched off using a razor blade, the measured ionic conductivities increased from $1 \cdot 10^{-5}$ S/cm to $9 \cdot 10^{-4}$ S/cm as depicted in Figure 5c.

For the thermoplastic samples, SEM micrographs showed a porous structure of the electrolyte after drying. The PVdF sample showed smaller and less amounts of pores, whereas the PVdF-HFP sample showed small, interconnected beads forming a polymer scaffold (cf. Figure a-d). After densification of both samples by hot-calendering, a dense and uniform layer is obtained with a smooth surface (cf. Figure 6 e-h).

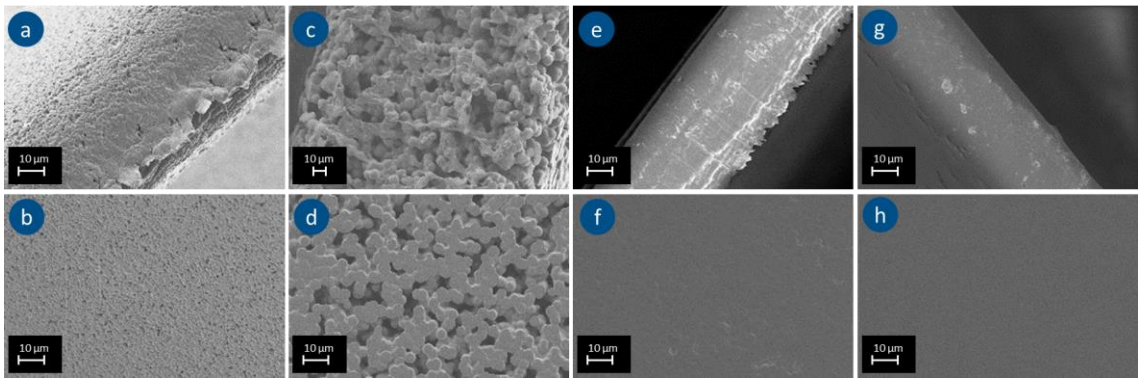

Figure 6: SEM micrographs of cross-sections (a,c,e,g) and surfaces (b,d,f,h) of the electrolyte films before (a-d) and after (e-h) hot-calendering, using thermoplastic polymers. a,b,e,f PVdF mixed with 70 vol.% of 1M LiTFSI in $PYR_{13}FSI$, c,d,g,h PVdF-HFP mixed with 70 vol.% 1M LiTFSI in $PYR_{13}FSI$.

Several parameters can affect the resulting morphologies of the thermoplastic electrolyte films after drying, including specific interactions with the Li salt and ionic liquid [18, 19], as well as exposure to moisture [20]. Clearly, the chemical “inertness” of fluorinated polymers, as they are often regarded [21], cannot be verified for this system and a complex interplay between the ILE, the NMP solvent, as well as residual moisture can all affect the resulting film morphology.

For both electrolyte classes, i.e. with thermoset and thermoplast, a strong interaction between the polymer and the ILE could be observed. To further characterize this behavior, DSC measurements were conducted (cf. Figure 7). First the thermoset mixture Araldite LY556/ XB3473 was measured starting from -30°C to 200°C. A broad exothermic peak could be observed between 100°C and 200°C, corresponding to the curing reactions which are expected to lie in the range of 120-220°C according to

the recommended curing procedures stated in the data sheet. Then a mixture of the thermoset and the ILE (0.2 LiTFSI- 0.2 $PYR_{13}TFSI$- 0.6 $PYR_{13}FSI$; 65 wt.%) was measured using the same measuring procedure (cf. Figure 7a). Due to the lower amount of thermoset material in this sample, the intensity of the resulting peak for the curing reaction of the thermoset was lower. However, the peak maximum also shifted towards lower values and was observed at around 110°C compared to 170°C for the pristine thermoset mixture. Therefore, a catalytic effect of the ILE on the curing reactions of the thermoset material could be verified. The catalytic effect of Lewis-acids (e.g. Li^+) on the polymerization of thermoset materials is well established [22, 23] and can be assumed to be responsible for the shift of the polymerization reactions towards lower temperatures.

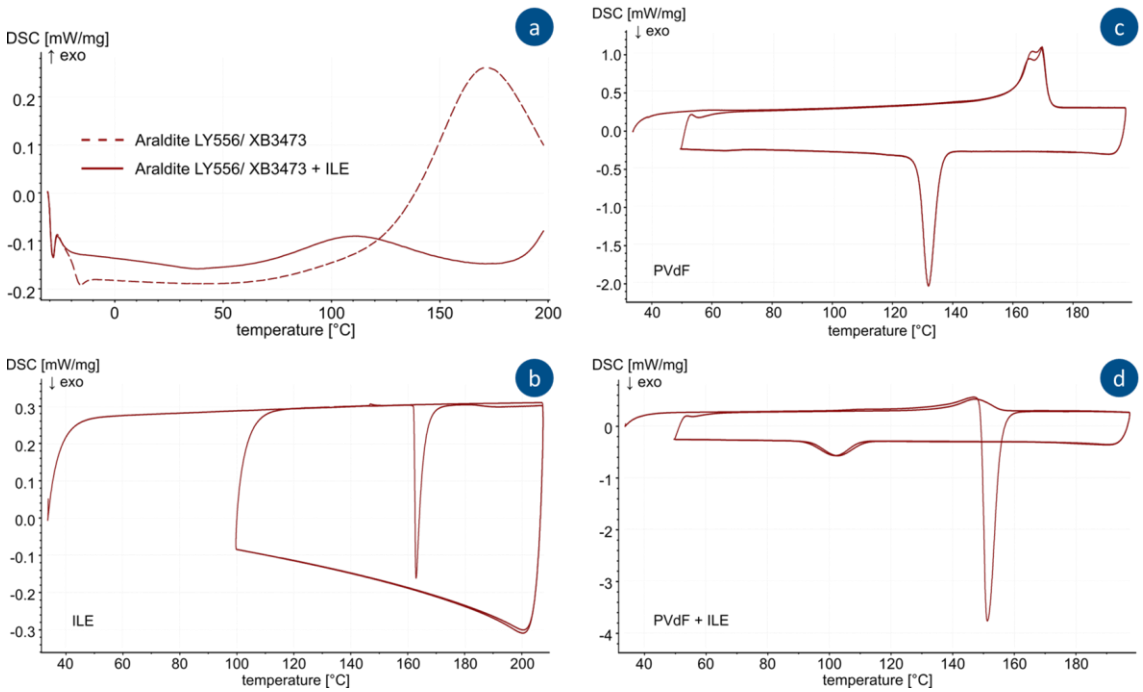

Figure 7: DSC signals of a, Araldite LY556/ XB3473 with and without ILE, b, PVdF (pristine), c, the ILE (1M LiTFSI in $PYR_{13}FSI$), and d, the electrolyte film using PVdF and 70 vol.% of the ILE.

For the thermoplast-based electrolyte films, first the PVdF polymer, then the pristine ILE and finally a mixture of both (electrolyte film after calendering) was measured between 30°C and 200°C. The DSC data is presented in Figure 7b-d respectively. PVdF shows an endothermic peak centered around 170°C, well in line with the expected melting range of the polymer. During cooling an exothermic peak at 130°C is observed, indicating re-crystallization of the polymer. Otherwise, no further reaction could be observed. The ILE (1M LiTFSI in $PYR_{13}FSI$) showed an exothermic peak close to 160°C, which is only observed for the first heating step. During cooling of the sample, no corresponding peak could be seen, indicating a non-reversible reaction. When the same sample is heated again, no further peaks are observed and only a flat baseline is observed. A highly exothermic reaction was reported for FSI^- anions in combination with Li^+ and residual moisture in the range between 120°C to 185°C, depending on the moisture content of the sample [24, 25]. It is assumed that the S-N bonds of the FSI^- anion decompose and that $FSO_2N^{\cdot}$·radicals are forming. In addition, this decomposition reaction leads to a Li^+ deficiency in the ILE and thus reduces the ionic conductivity [24]. The dry room conditions under which the electrolyte films are prepared might not suffice to fully avoid the exothermic reaction of FSI^- as already low amounts of H_2O can trigger it. For the electrolyte films using PVdF and the ILE, the melting range of the polymer component is shifted towards lower temperature, showing a maximum at 150°C. This further verifies a change in the polymer due to interactions with the ILE and might indicate a plasticizing

effect of the latter on the system. Furthermore, the exothermic reaction observed for the pristine ILE is also observed for the thermoplast-based electrolyte. The onset of the reaction, however, is decreased to 150°C. Thermoplast electrolyte samples heated at 150°C for one hour turned yellowish, and showed reduced ionic conductivity by almost one order of magnitude; verifying decomposition of FSI^-.

Clearly, the thermal analysis studies for the thermoset as well as thermoplastic electrolytes verified the conclusions drawn from the SEM micrographs. Pronounced interactions between the polymeric components and the ILE are observed, leading to different physico-chemical properties than expected from non-reactive mixtures thereof.

3.3 mechanical testing

In order to determine the mechanical stability of the prepared electrolyte layers, tensile testing was used on the thermoplast-electrolyte samples. Due to the limited mechanical stability of the thermoset samples when thin sheets were prepared, no tensile testing could be performed for these samples. The Young's modulus of PVdF and PVdF-HFP should be in the range of 1-2 GPa [26, 27], whereas the tested samples with 70 vol.% of the ILE showed values of only 60 MPa and 10 MPa for PVdF and PVdF-HFP, respectively (cf. Figure 8a). Reducing the ILE content to 60 vol.%, though, significantly increased the mechanical stability and Young's moduli of 162 MPa could be obtained for samples using PVdF.

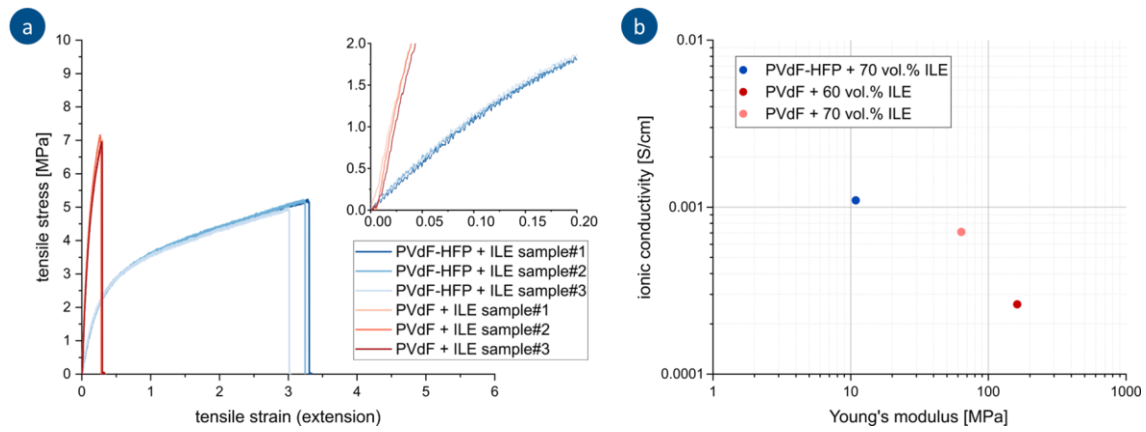

Figure 8: Tensile test (a) of thermoplast samples using PVdF-HFP (blue) and PVdF (red). For each material, three different samples were tested; (b) ionic conductivity vs. Young's modulus plot for thermoplast samples.

The reduction of Young's modulus of the polymer material with addition of the ILE can be estimated by using theoretical models which calculate the reduction in Young's modulus with porosity. Most of the applicable models yield a reduction of 80-90% in the Young's modulus [28] for porosities of 60-70%. For pristine PVdF and PVdF-HFP a Young's modulus of 1-2 GPa can be assumed and thus for the thermoplast electrolytes using 60 vol.% and 70 vol.% ILE a Young's modulus of around 200-400 MPa and 100-200 MPa can be expected, respectively. The measured values, though, are considerably lower compared to the expected ones. The interactions between the polymer and the ILE are assumed to heavily reduce the mechanical properties of the polymers, yielding lower than expected mechanical strength. Nevertheless, a significant difference can be seen in the Young's modulus of the two different thermoplast materials. Samples using PVdF seem to be less affected by the ILE compared to the PVdF-HFP samples. At the same time, though the ionic conductivity seems to be less affected by addition of PVdF-HFP compared to PVdF (cf. Figure 8b). This observations highlight the critical need to further understand the chemical interactions between the lithium ion conducting and mechanically reinforcing component of multifunctional electrolytes.

9 CONCLUSIONS

In this work two different approaches for preparation of multifunctional electrolytes have been investigated and compared with each other. An ionic liquid electrolyte with high safety and feasible ionic conductivity was employed for the preparation of either a biphasic system using thermoset materials as mechanically reinforcing component, or a monophasic electrolyte for which thermoplast materials have been dissolved into the liquid electrolyte. Thus, two types of multifunctional electrolytes were obtained. It could be shown by SEM and DSC analyses, that both approaches suffer from interactions between the reinforcing polymers and the ionic liquid electrolyte, yielding lower than expected mechanical properties and ionic conductivities. For the thermoset samples, a strong dependence of the resulting polymer morphology and curing behavior on the used ionic liquid electrolyte was observed. In addition, a *skin-effect*, i.e. a surface layer of the thermoset material on the electrolyte film which showed lower porosity than the bulk material, inhibited proper ionic conduction. The thermoplast electrolytes showed a porous structure after casting and drying of the films, indicating repulsive interactions between the selected polymers and ionic liquid electrolytes. Furthermore, the melting behavior of the polymer changed when mixed with the ionic liquid electrolyte. Nevertheless, the straightforward processing of these materials rendered them superior compared to their thermoset counterparts. Finally, ionic conductivities of around $1 \cdot 10^{-3}$ S/cm and Young's moduli of 60 MPa could be reached. Further mechanical reinforcement of the electrolytes will be required to increase their multifunctional nature. Advances in solid electrolytes, especially in ion-conducting ceramics, might enable higher mechanical strength by preparation of monophasic thermoplast electrolytes with ceramic fillers. These fillers can act as mechanically reinforcements and at the same time could contribute to the lithium ion conduction. However, the complex physico-chemical interactions of the employed materials need to be further investigated first to properly understand and anticipate their impact on the electrochemical and mechanical performance.

ACKNOWLEDGEMENTS

This review was prepared within the project SOLIFLY that received funding from the Clean Sky 2 Joint Undertaking (JU) under grant agreement No. 101007577.

REFERENCES

[1] K.K. Sairajan, G.S. Aglietti and K.M. Mani, A review of multifunctional structure technology for aerospace applications, *Acta Astronautica*, ***120***, 2016, pp. 30-42 (http://dx.doi.org/10.1016/j.actaastro.2015.11.024).

[2] F. Danzi, R.M. Salgado, J.E. Oliveira, A. Arteiro, P.P Camanho and M.H. Braga, Structural batteries: A review, *Molecules*, ***26***, 2021, pp. 2203 (https://doi.org/10.3390/molecules26082203).

[3] H. Kühnelt, A. Beutl, F. Mastropierro, F. Laurin, S. Willrodt, A. Bismarck, M. Guida and F. Romano, Structural batteries for aeronautic applications – State of the art, research gaps and technology development needs, *Aerospace*, ***9***, 2022, pp. 7 (https://doi.org/10.3390/aerospace9010007).

[4] A. Sheidaei, X. Xiao, X. Huang and J. Hitt, Mechanical behavior of a battery separator in electrolyte solutions, *Journal of Power Sources*, ***196***, 2011, pp. 8728-8734 (https://doi.org/10.1016/j.jpowsour.2011.06.026).

[5] J. Cannarella, X. Liu, C.Z. Leng, P.D. Sinko, G.Y. Gor and C.B. Arnold, Mechanical properties of a battery separator under compression and tension, *Journal of The Electrochemical Society*, ***161***, 2014, pp. F3117-F3122 (DOI 10.1149/2.0191411jes).

[6] V. Tu, L.E. Asp, N. Shirshova, F. Larsson, K. Runesson and R. Jänicke, Performance of bicontinuous structural electrolytes, *Multifunctional Materials*, ***3***, 2020, pp. 025001 (DOI 10.1088/2399-7532/ab8d9b).

[7] S.J. Kwon, T. Kim, B.M. Jung, S.B. Lee and U.H. Choi, Multifunctional epoxy-based solid polymer electrolytes for solid-state supercapacitors, *ACS Appl. Mater. Interfaces*, ***10***, 2018, pp. 35108-35117 (https://doi.org/10.1021/acsami.8b11016).

[8] B. Demir, K.-Y. Chan and D.J. Searles, Structural electrolytes based on epoxy resins and ionic liquids: A molecular-level investigation, *Macromolecules*, ***53***, 2020, pp. 7635-7649 (https://doi.org/10.1021/acs.macromol.0c00824).

[9] K. Sakakibara, H. Kagata, N. Ishizuka, T. Sato and Y. Tsujii, Fabrication of surface skinless membranes of epoxy resin-based mesoporous monoliths toward advanced separators for lithium ion batteries, *Journal of Materials Chemistry A*, ***5***, 2017, pp. 6866-6873 (https://doi.org/10.1039/C6TA09005B).

[10] J. Xu, Z. Geng, M. Johansen, D. Carlstedt, S. Duan, T. Thiringer, F. Liu and L.E. Asp, A multicell structural battery composite laminate, *EcoMat*, ***4***, 2022, pp. e12180 (https://doi.org/10.1002/eom2.12180).

[11] N. Shirshova, A. Bismarck, E.S Greenhalgh, P. Johansson, G. Kalinka, M.J. Marczewski, M.S.P. Shaffer and M. Wienrich, Composition as a means to control morphology and properties of epoxy based dual-phase structural electrolytes, *J. Phys. Chem. C*, ***118***, 2014, pp. 28377-28387 (https://doi.org/10.1021/jp507952b).

[12] P. Liu, E. Sherman and A. Jacobsen, Design and fabrication of multifunctional structural batteries, *Journal of Power Sources*, ***189***, 2009, pp. 646-650 (https://doi.org/10.1016/j.jpowsour.2008.09.082).

[13] S. Ekstedt, M. Wysocki and L.E. Asp, Structural batteries made from fibre reinforced composites, *Macromolecular Engineering*, ***39***, 2010, pp. 148-150 (https://doi.org/10.1179/174328910X12647080902259).

[14] J.F. Snyder, E.D. Wetzel and C.M. Watson, Improving multifunctional behavior in structural electrolytes through copolymerization of structure- and conductivity-promoting monomers, *Polymer*, ***50***, 2009, pp. 4906-4916 (https://doi.org/10.1016/j.polymer.2009.07.050).

[15] D. Vogt, P. Michalowski and A. Kwade, Production and characterisation of fibre-reinforced all-solid-state electrodes and separator for the application in structural batteries, *Batteries*, ***8***, 2022, pp. 55 (https://doi.org/10.3390/batteries8060055).

[16] M. Moreno, E. Simoentti, G.B. Appetecchi, M. Carewska, M. Montanino, G.-T. Kim, N. Loeffler and S. Passerini, Ionic liquid electrolytes for safer lithium batteries, *Journal of The Electrochemical Society*, ***164***, 2017, pp. A6026-A6031 (DOI 10.1149/2.0051701jes).

[17] J. Landesfeind, J. Hattendorff, A. Ehrl, W.A. Wall and H.A. Gasteiger, Tortuosity determination of battery electrodes and separators by impedance spectroscopy, *Journal of The Electrochemical Society*, ***163***, 2016, pp. A1373-A1387 (DOI 10.1149/2.1141607jes).

[18] T. Lestariningsih, Q. Sabrina, C.R. Ratri, A. Subhan and S. Priyana, The effect of LiBOB addition on solid polymer electrolyte (SPE) production based PVDF-HFP/TiO2/LiTFSI on ionic conductivity for lithium-ion battery applications, *Jurnal Kimia Sains dan Aplikasi*, ***25***, 2022, pp. 13-19 (https://doi.org/10.14710/jksa.25.1.13-19).

[19] R. Gonçalves, D. Miranda, A.M. Almeida, M.M. Silva, J.M. Meseguer-Dueñas, J.L. Gomez Ribelles, S. Lanceros-Méndez and C.M. Costa, Solid polymer electrolytes based on lithium bis(trifluoromethanesulfonyl)imide/poly(vinylidene fluoride-co-hexafluoropropylene) for safer rechargeable lithium-ion batteries, *Sustainable Materials and Technologies*, ***21***, 2019, pp. e00104 (https://doi.org/10.1016/j.susmat.2019.e00104).

[20] M. Li, I. Katsouras, C. Piliego, G. Glasser, I. Lieberwirth, P.W.M. Blom and D.M. de Leeuw, Controlling the microstructure of poly(vinylidenefluoride) (PVDF) thin films for microelectronics, *J. Mater. Chem. C*, ***1***, 2013, pp. 7695 (https://doi.org/10.1039/C3TC31774A).

[21] J.E. Marshall, A. Zhenova, S. Roberts, T. Petchey, P. Zhu, C.E.J. Dancer, C.R. McElroy, E. Kendrick and V. Goodship, On the solubility and stability of polyvinylidene fluoride, *Polymers*, ***13***, 2021, pp. 1354 (https://doi.org/10.3390/polym13091354).

[22] T. Vidil, F. Tournilhac, S. Musso, A. Robisson and L. Leibler, Control of reactions and network structures of epoxy thermosets, *Progress in Polymer Science*, ***62***, 2016, pp. 126-179 (https://doi.org/10.1016/j.progpolymsci.2016.06.003).

[23] T. Hansen, P. Vermeeren, R. Yoshisada, D.V. Filippov, G.A. van der Marel, J.D.C. Codée and T.A. Hamlin, How Lewis acid catalyze ring-openings of cyclohexene oxide, *J. Org. Chem.*, ***86***, 2021, pp. 3565-3573 (https://doi.org/10.1021/acs.joc.0c02955).

[24] J. Huang and F. Hollenkamp, Thermal behavior of ionic liquids containing the FSI anion and the Li^+ cation, *J. Phys. Chem. C,* ***114***, 2010, pp. 21840-21847 (https://doi.org/10.1021/jp107740p).

[25] M. Kerner, N. Plyahan, J. Scheers and P. Johansson, Thermal stability and decomposition of lithium bis(fluorosulfonyl)imide (LiFSI) salts, *RSC Adv.*, ***6***, 2016, pp. 23327 (https://doi.org/10.1039/C5RA25048J).

[26] Y. Shu, L. Ke, J. Su and F. Shen, Experimental studies on fretting wear behavior of PVDF piezoelectric thin films, *Materials*, ***14***, 2021, pp. 734 (DOI: 10.3390/ma14040734).

[27] Q. Chen, D. Natale, B. Neese, K. Ren, M. Lin and Q.M. Zhang, Piezoelectric polymers actuators for precise shape control of large scale space antennas, *Proc. SPIE 6524, Electroactive Polymer Actuators and Devices (EAPAD) 2007, 65241P (5 April 2007)* (https://doi.org/10.1117/12.717696).

[28] J.A. Choren, S.M. Heinrich and M.B. Silver-Thorn, Young's modulus and volume porosity relationships for additive manufacturing applications, *J. Mater. Sci.,* ***48***, 2013, pp. 5103-5112 (https://doi.org/10.1007/s10853-013-7237-5).